Optical Engineering

SPIEDigitalLibrary.org/oe

Acceleration of split-field finite difference time-domain method for anisotropic media by means of graphics processing unit computing

Jorge Francés
Sergio Bleda
Mariela Lázara Álvarez
Francisco Javier Martínez
Andres Márquez
Cristian Neipp
Augusto Beléndez

Optical Engineering 53(1), 011005 (January 2014)

Acceleration of split-field finite difference time-domain method for anisotropic media by means of graphics processing unit computing

Jorge Francés
Sergio Bleda
Mariela Lázara Álvarez
Alicante University/San Vicente del Raspeig Drive
Department of Physics, Systems Engineering and Signal Theory
San Vicente del Raspeig
Alicante 3080, España
and
Alicante University/San Vicente del Raspeig Drive
University Institute of Physics to Sciences and Technologies
San Vicente del Raspeig
Alicante 3080, España
E-mail: jfmonllor@ua.es

Francisco Javier Martínez
Alicante University/San Vicente del Raspeig Drive
Department of Physics, Systems Engineering and Signal Theory
San Vicente del Raspeig
Alicante 3080, España

Andres Márquez
Cristian Neipp
Augusto Beléndez
Alicante University/San Vicente del Raspeig Drive
Department of Physics, Systems Engineering and Signal Theory
San Vicente del Raspeig
Alicante 3080, España
and
Alicante University/San Vicente del Raspeig Drive
University Institute of Physics to Sciences and Technologies
San Vicente del Raspeig
Alicante 3080, España

Abstract. The implementation of split-field finite difference time domain (SF-FDTD) applied to light-wave propagation through periodic media with arbitrary anisotropy method in graphics processing units (GPUs) is described. The SF-FDTD technique and the periodic boundary condition allow the consideration of a single period of the structure reducing the simulation grid. Nevertheless, the analysis of the anisotropic media implies considering all the electromagnetic field components and the use of complex notation. These aspects reduce the computational efficiency of the numerical method compared with the isotropic and nonperiodic implementation. Specifically, the implementation of the SF-FDTD in the Kepler family of GPUs of NVIDIA is presented. An analysis of the performance of this implementation is done, and several applications have been considered in order to estimate the possibilities provided by both the formalism and the implementation into GPU: binary phase gratings and twisted-nematic liquid crystal cells. Regarding the analysis of binary phase gratings, the validity of the scalar diffraction theory is evaluated by the comparison of the diffraction efficiencies predicted by SF-FDTD. The analysis for the second order of diffraction is extended, which is considered as a reference for the transmittance obtained by the SF-FDTD scheme for periodic media. [DOI: 10.1117/1.OE.53.1.011005]

Subject terms: split-field finite difference time domain; graphics processing unit computing; anisotropic media; diffraction efficiency; polarization gratings; binary phase gratings.

Paper 130560SSP received Apr. 12, 2013; revised manuscript received Jul. 9, 2013; accepted for publication Aug. 1, 2013; published online Aug. 28, 2013.

1 Introduction

It has been demonstrated that the finite difference time-domain (FDTD) method is an extremely important numerical method for solving Maxwell's equations. Since 1966, when Yee proposed the basis of this numerical method, there have been a great number of contributions focused on extending its capabilities for modeling new applications.

Nonetheless, the potential of this method had not been massively exploited till 1980s and 1990s, when the performance of modern computers began to rise following the well-known Moore's law. The number of contributions related to FDTD has increased dramatically in the last 20 years due to the possibility of modeling complex structures easily with standard computers. Many authors focused their attention in the application of FDTD to periodic media. These kinds of arrangements are usual in optical applications such as liquid crystal light valves and photonic wave guides, for instance. The scheme proposed for modeling accurately these kinds of problems is known as the split-field FDTD (SF-FDTD)[1,2] formulation. This theory describes an efficient scheme for modeling light-wave propagation through periodic media by means of FDTD. Recently, SF-FDTD implementation schemes for anisotropic media in two and three dimensions have been detailed in Refs. 3 and 4.The adapting capability of FDTD makes it easier to simulate complex structures compared with purely analytic methods that hardly provide closed expressions for these situations.

However, modeling optical elements with anisotropic dielectric properties, such as waveplates and liquid crystal light valves, implies considering a full-tensor description of the relative dielectric permittivity. On the other hand,

0091-3286/2014/$25.00 © 2014 SPIE

for correctly applying the periodic boundary conditions (PBCs) for an arbitrary angle of incidence, it is necessary to consider the complex notation of the electromagnetic field. In terms of computer resources, this issue implies an increased factor of 2 in the memory usage. The number of operations is also increased, since real and imaginary parts of the fields must be considered. All these aspects reduce the performance of SF-FDTD in terms of computational resources and time simulation.

In the last years, many scientific areas are taking advantage of the general purpose graphics processing units (GPUs) based on the compute-unified device architecture (CUDA).[5,6] The analysis of complex systems in many cases requires massive computations that makes the processing by means of modern workstations unaffordable. Many authors are focusing their efforts on how to adapt the implementation of numerical methods under the CUDA compliance. Some examples can be found in literature for different topics such as physics,[7,8] astronomy,[9,10] images,[11–13] biomedical applications,[14,15] and computer science.[16] The acceleration of the SF-FDTD by means of GPU computing has recently been introduced by Shahmansouri et al.[17] In their work, GPU computing is applied to accelerate the SF-FDTD implementation for Drude-Lorentz dispersive media. Nevertheless, the analysis of anisotropic media and GPU computing has not been performed to the best of our knowledge. Here, a parallel implementation of SF-FDTD for anisotropic media is detailed and compared with the sequential version that runs under a single CPU. Considering anisotropy and a full-tensor formulation for the dielectric permittivity implies more computer resources.

First, the isotropic version for both CPU and GPU are applied to the analysis of the diffraction efficiency of dielectric binary gratings. Dielectric binary gratings are of wide interest owing to their many applications in polarization systems,[18] solar energy,[19,20] ultrafast optics,[21] displays,[22] and coherence.[23] Several investigators analyze the grating properties in the frame of scalar optics.[24,25] Simplified theories are commonly used and are attractive in the design and analysis of the diffractive optical elements (DOEs) because of their simplicity and low-computational intensity.[26,27] Thanks to the spectacular improvements in grating manufacturing in the middle of the century,[28,29] it has become possible to achieve high-quality gratings with more than 1000 lines/mm.[30] Here, the groove spacing and the wavelength became of the same order of magnitude, and it has been demonstrated that there exists a clear influence of polarization on the efficiency curves. Therefore, taking into account the vectorial character of light became evident. For highly spatial frequency gratings, the wavelength-to-period ratio is large enough so that all nonzero diffracted orders are cut-off. In this scenerio, the effective medium theory (EMT) has extensively been used, due to its capability of modeling a subwavelength grating as an anisotropic optical thin film with effective refractive indices. There are several works[31–33] that are focused on determining the reliability of EMT for some DOEs. However, for diffractive phase elements (DPEs) with feature sizes much greater than the wavelength of the incident light, the scalar diffraction theory (SDT) is more accurate than EMT. The accuracy of SDT has previously been compared with the rigorous-coupled wave (RCW) theory in the works by Pommet et al.,[34] Glytsis et al.,[35] and also for perfectly conducting gratings in Ref. 36 among others. Regarding dielectric DPEs, the reliability of SDT results for the zero- and first-diffraction orders has been analyzed as a function of the normalized thickness (h/λ) in a specific range for different periods and illumination schemes. However, the higher orders were not taken under consideration. Recently, Jing et al.[37] presented a deep analysis of the accuracy of both the SDT and the EMT for analyzing the transmittance characteristics of diffraction phase gratings at normal incidence. The results derived from Ref. 37 conclude that the SDT can accurately estimate the diffraction efficiency even with periods of two wavelengths ($\Lambda/\lambda = 2$) under several conditions. Here, the analysis of Jing et al. has been corroborated and extended to the second order of diffraction considering as rigorous EM theory, the novel SF-FDTD scheme.

Second, the anisotropic version of the SF-FDTD is implemented for GPU computing and also validated by means of the analysis of a polarization grating. In both cases, the normal and the oblique incidence is considered for the validation of our implementation. The model of this system gives us the opportunity of simulating a wide range of devices such as those based on a twisted-nematic liquid crystal (TN-LC), parallel-aligned liquid crystal on silicon (LCoS), or optical activity cavities. Many optical phenomena of optical materials are anisotropic[38] such as nonlinear effects, cross-phase modulation,[39] cross-absorption modulation,[40] and four-wave mixing,[41,42] for instance. These effects have successfully been utilized in a wide range of photonic applications including lasers, amplifiers, switchers, modulators, and all-optical logic gates[38,43,44] among others. Thus, we investigate the performance of the SF-FDTD for anisotropic media due to the impact of optical anisotropy in optical devices. The degree of improvement of the GPU code is compared with the sequential version in terms of the relative SpeedUp, which is defined as the difference between the sequential and the parallel time simulations. This analysis has been performed for both scenarios isotropic and anisotropic media in order to demonstrate the possibilities offered by GPU computing in cases that imply massive computations.

2 SF-FDTD Theory

The standard FDTD scheme was previously applied to DOEs with succesful results in Refs. 45 and 46. Although FDTD belongs to the rigorous EM theory,[47] the spatial discretization of the DPE limits the number of periods of the DPE, and thus an infinite plane of incidence can not be considered. This issue must be taken under consideration when the FDTD results are compared with rigorous coupled wave analysis (RCWA) for instance, in which the plane of incidence is considered infinitely extent. This topic has been analyzed in Refs. 45, 46, and 48. In this work, the SF-FDTD scheme with PBCs has been applied in order to avoid the drawbacks mentioned below, since the simulation of a single-unit cell of the periodical DOE can be performed providing precise prediction of the electromagnetic field.[2,3,47]

In this work, Maxwell's equations for nonconducting and nonmagnetic anisotropic medium in phasor form are considered.

$$j\omega\epsilon_0\mathbf{E} = \kappa\nabla\times\mathbf{H}, \tag{1}$$

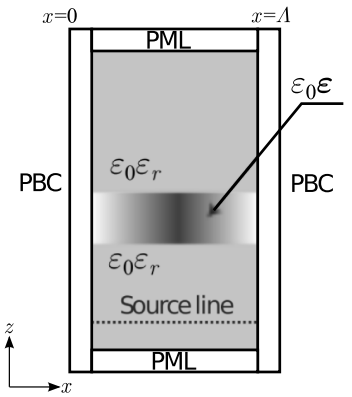

Fig. 1 General problem space for FDTD simulations used in this work. The boundaries of the periodic media are established at $x = 0$ and $x = \Lambda$, where Λ is the period of the structure.

$$j\omega\mu_0\mathbf{H} = -\nabla \times \mathbf{E}, \tag{2}$$

where ω is the angular frequency and ϵ_0 and μ_0 are the permittivity and the permeability of free space, respectively. For convenience, the impermittivity tensor e $\kappa = \epsilon^{-1}$ is introduced instead of ϵ, which is defined as

$$\epsilon = \begin{bmatrix} \epsilon_{xx} & \epsilon_{xy} & \epsilon_{xz} \\ \epsilon_{yx} & \epsilon_{yy} & \epsilon_{yz} \\ \epsilon_{zx} & \epsilon_{zy} & \epsilon_{zz} \end{bmatrix} = \mathbf{T}^{-1}(\alpha,\beta,\gamma) \begin{bmatrix} \epsilon_1 & 0 & 0 \\ 0 & \epsilon_2 & 0 \\ 0 & 0 & \epsilon_3 \end{bmatrix} \mathbf{T}(\alpha,\beta,\gamma), \tag{3}$$

where $\epsilon_{1,2,3}$ are the relative dielectric constants corresponding to the principal axes, $\mathbf{T}$ is the transformation matrix fully detailed in Ref. 3, and α, β, and γ are the Euler angles.[49]

In the SF formulation plane, waves propagate along a periodic structure with an angle of incidence θ_0. The scheme of simulation is illustrated in Fig. 1.

By means of the wave-vector $\mathbf{k}$, the new field variables $\mathbf{P}$ and $\mathbf{Q}$, which implicitly contain the oblique-field propagation, are defined as

$$\mathbf{P} = \mathbf{E} \exp(jk_x x), \tag{4}$$

$$\mathbf{Q} = c\mu_0\mathbf{H} \exp(jk_x x), \tag{5}$$

where c is the speed of light in free space and $k_x = (\omega/c)\sin\theta_0$. Substituting Eqs. (4) and (5) into Eqs. (1) and (2), the expressions of each component can be obtained and discretized following the center difference expressions for both time and spatial derivatives.[3,4]

3 GPU Implementation of the SF-FDTD

Here, a GTX670 GPU is considered for the parallel implementation of the SF-FDTD for anisotropic media. This GPU belongs to the Kepler architecture released by NVIDIA in the Spring of 2012. Kepler's memory hierarchy is organized similar to Fermi. The Kepler architecture supports a unified memory request path for loads and stores it with an L1 cache per SMX multiprocessor. The Kepler GTX670 features 1344 CUDA cores organized in seven SMX units. Each SMX has a fully pipelined floating point and integer arithmetic logic units retaining the architecture introduced in Fermi. Each SMX also has a block of local memory called shared memory that is visible to all threads within a thread block, and a set of scheduling units used to schedule warps, and the basic computing unit that consists of 32 threads. The GPU is capable of swapping warps into and out of context without any performance overhead. This functionality provides an important method of hiding memory and instruction latency on the GPU hardware.

To ease the mapping of data to threads, the threads identifiers may be multidimensional and, since a very high number of threads run in parallel, CUDA groups threads in blocks and grids. One of the crucial requirements to achieve a good performance on the NVIDIA GPU is to hide the high latency of the global memory ensuring coalesced memory accesses.

Therefore, concerning the architecture of the GPU is mandatory to be successful in GPU computing. Regarding the SF-FDTD implementation in the GPU, it must be said that a number of blocks related to the number of rows and columns are invoked by means of the kernel functions, and an array of 192×2 threads are launched per block. This scheme is illustrated in Fig. 2(a), in which a detail of the threads and their arrangement inside the grid of blocks is shown. Besides the potential of the CUDA kernel, it is necessary to divide the whole computation process into several kernels focused on computing each component of the electromagnetic field. Figure 2(b) summarizes the invocation path of the kernels related with the SF-FDTD implementation. In this flow chart, the postprocess is omitted, but mandatory downloads of the $\mathbf{P}$ and $\mathbf{Q}$ components must be considered in order to compute the desired specific outputs such as diffraction efficiencies or Stokes parameters.

It is interesting to note that with GPU computing, each thread being executed in GPU can be in charge of updating a single position of the SF-FDTD grid. This strategy is slightly different from that commonly used by traditional CPUs, in which a single thread performs a set of loops in order to update the entire SF-FDTD grid. The best block size and the optimal arrangement of the CUDA threads were defined by means of an experimental procedure based on the scheme proposed in Ref. 50 for the standard FDTD scheme. First, all the constant parameters, such as the permittivity tensor, are uploaded to the GPU global memory. Second, all memory needed for storing the $\mathbf{Q}$ and $\mathbf{P}$ fields is allocated in the GPU global memory. Third, for each time step, a set of kernels is invoked in order to solve each field component. The segmentation of the kernels is based on updating each electromagnetic component by means of a grid of blocks. This arrangement improves the efficient use of the shared memory in the device and also the correct usage of the cache. This effect was improved in Fermi architecture, where each SMX has 64 KB of on-chip memory that can be configured as 48 KB of shared memory with 16 KB of L1 cache or as 16 KB of shared memory with 48 KB of L1 cache. Nonetheless, applications that do not use shared memory automatically benefit from the L1 cache allowing high performance CUDA programs to be built with minimum time

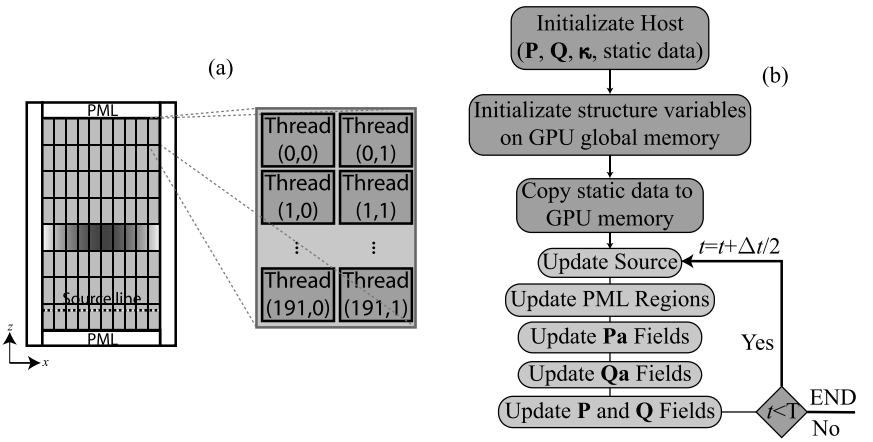

Fig. 2 (a) Arrangement scheme of the grid of blocks invoked by compute-unified device architecture (CUDA) Kernels with a detail of the threads that conform each block. (b) Flowchart of graphics processing unit (GPU) parallel programming for split-field finite difference time-domain (SF-FDTD).

and effort. Finally, the results derived from the simulation are downloaded to the host memory by means of the PCI express bus, in order to be used for the CPU and the main application. This scheme is based on the same way of updating the electromagnetic field for the standard FDTD scheme fully detailed in Ref. 50.

4 Results

In this section, the validation results of the implementation described here are summarized. This validation is done for both the isotropic and the anisotropic version. The systems simulated are based on the analysis performed in Refs. 3 and 51. In all cases, the software runs under a Unix-based platform with an Intel Xeon E5-2630 processor with 15 MB of cache, a clock speed of 2.3 GHz, and 16 GB of global DDRAM3. Regarding the GPU, all the computations are processed by a NVIDIA GTX-670 card.

4.1 *Accuracy Analysis of the Scalar Diffraction Theory*

In Fig. 3, Λ and h represent the period and the groove depth, respectively, and n_0 and n_g are the refractive indices of the incident medium and the grating, respectively. The light wave propagates from air ($n_0 = 1.00$) through the surface into the substrate material ($n_g = 1.50$). The scalar diffraction efficiency can be calculated by using the scalar Kirchhoff diffraction theory, which neglects the vectorial and the polarized nature of light. This theory provides reasonably accurate results when the periodicity of the surface profile is much larger than the wavelength of the incident light.[37] Specifically, when $\Lambda/\lambda \geq 20$, physical optics according to Fresnel and Snell's laws can explain the behavior of the diffraction efficiency of these optical elements.[37,52]

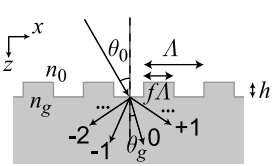

Fig. 3 Scheme of a diffraction phase grating.

This simplified theory is based on the general equation for diffraction efficiency η in scalar approximation for a periodic structure as[37,53]

$$\eta(\lambda) = \left| \frac{1}{\Lambda} \int_0^{\Lambda} t(x) e^{-2j\pi m x/\Lambda} \mathrm{d}x \right|^2, \tag{6}$$

where $t(x)$ is a function defined as the ratio of transmitted- (or reflected) and incident-wave amplitudes at location x and m is the diffracted order. Taking Eq. (6) into account and the geometry of the problem fully detailed in Fig. 3, the diffraction efficiencies for the zero and the higher orders can be easily derived[37,53]

$$\eta_0 = (n_g \cos\theta_g / n_0 \cos\theta_0)\tau^2(\theta_0) \times [1 - 2f(1-f)(1 - \cos\Delta\phi)], \tag{7}$$

$$\eta_{m\neq 0} = (n_g \cos\theta_g / n_0 \cos\theta_0)\tau^2(\theta_0)\{(1/m^2\pi^2) \times [1 - \cos(2m\pi f)](1 - \cos\Delta\phi)\}, \tag{8}$$

with θ_0 being the angle of incidence. The rays inside the grating have an angle respect to the x-axis θ_g that can be obtained via Snell's law. The Fresnel transmission coefficient is included by means of $\tau(\theta_0)$, and $\Delta\phi = 2\pi h/\lambda(n_g \cos\theta_g - n_0 \cos\theta_0)$ is the phase difference between two parallel rays incident on the grating at an angle θ_0.[37]

In order to show the potential of the SF-FDTD scheme, a set of binary gratings based on dielectric media is simulated. For illustrating this scheme, the E_y field has been represented in Fig. 4. In this example, the binary grating can be easily identified inside the grid simulation. The angle of incidence for this case is 30 deg, and the values of the FDTD parameters are listed in the table provided along with Fig. 4. The spatial and time resolutions are denoted by Δ and Δt, respectively, whereas R is the cells' density per wavelength.

In this section, the accuracy of SDT is analyzed through the SF-FDTD method as a reference. The SF-FDTD simulation parameters are listed in Table 1. In order to analyze the validity of the SDT, the diffraction efficiency of the 0th,

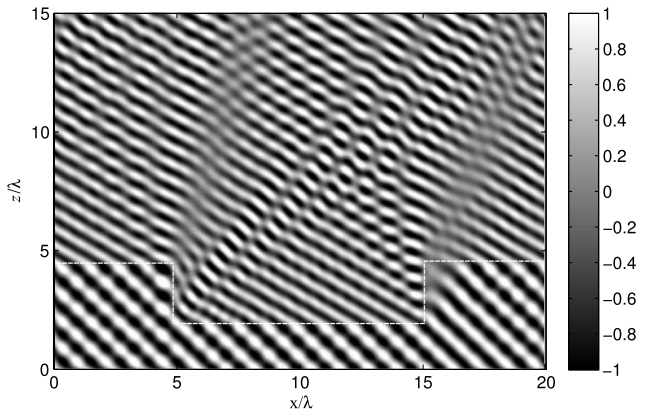

Fig. 4 Near-field image of the E_y field at 30 deg incidence. Parameters: $\Lambda = 3\lambda$, refractive index of $n_g = 1.5$, and output substrate is also a dielectric media of n_g.

Table 1 Split-field finite difference time-domain (SF-FDTD) parameters.

λ (nm)	Λ	Δ (nm)	Δt (ps)	R	Rows	Columns	Time steps
633	3λ	31.65	59.81	20	60	500	1200

$\pm$1st, and $\pm$2nd orders have been computed with both SDT and SF-FDTD as a function of the normalized depth and for different periods and duty cycles. These results are shown in Fig. 5 for both transverse electric (TE) and transverse magnetic (TM) polarizations. Regarding SDT and zeroth order, it can be seen that results for $h/\lambda = 0.5$ are slightly better than those obtained with $h/\lambda = 1$. This is due to the fact that the accuracy of SDT is improved when both the spatial frequency and the depth of the grating decrease. Therefore, the best results achieved for the zeroth order are in Figs. 5(a) and 5(j). For $h/\lambda = 1$, the zeroth-order converges more slowly to the SDT value. For the zeroth and first orders, the best results are for a fill factor of 0.5. There are small differences between TE and TM polarization, with TM polarization on a small scale being more accurate than TE.

For the first order, the results are quite similar identifying a wider region, in which the diffraction efficiency is close to the values established by SDT for $h/\lambda = 1$ in Figs. 5(b) and 5(e). For thicker gratings ($h/\lambda = 1$), the trend is similar but as mentioned below, the convergence of the SDT to FDTD curves is lower than those for thinner gratings. The most homogenous values of the diffraction efficiency are obtained also with $f = 0.5$. As can be seen in Figs. 5(e) and 5(k), for both normalized depths, the best results are achieved with TM polarization. This behavior can also be applied to the second order that is less energetic than the zeroth and first orders. However, the fact that SDT provides more precise predictions for first and second orders is corroborated.

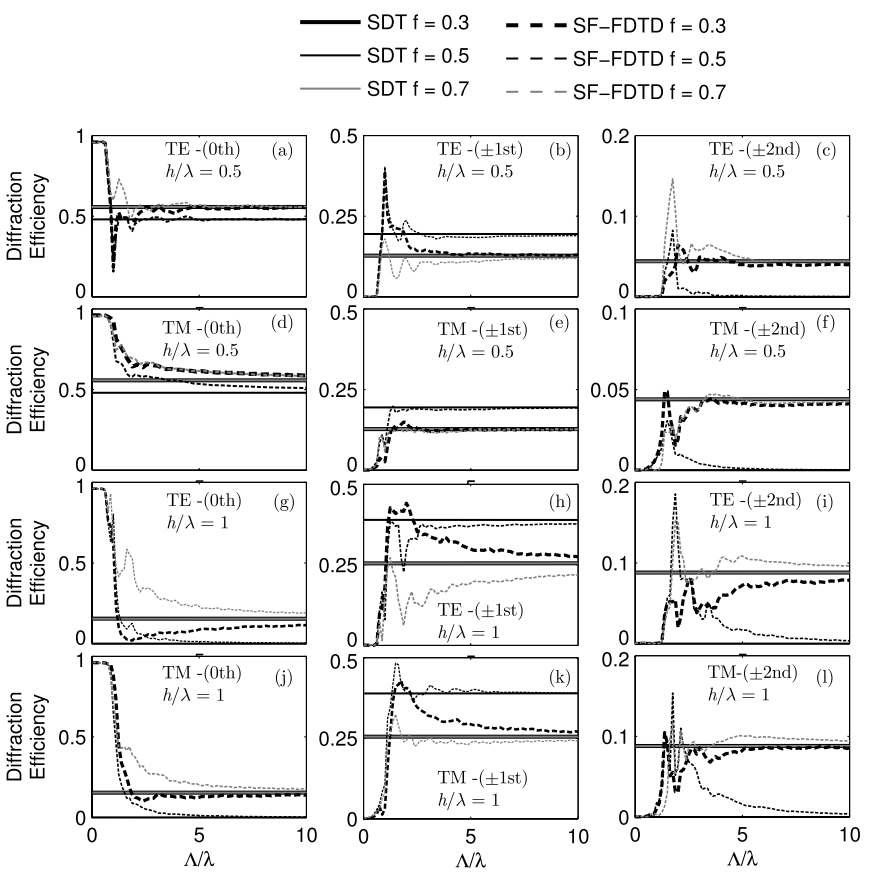

Fig. 5 Comparison of diffraction efficiencies between scalar diffraction theory (SDT), effective medium theory (EMT), and FDTD versus the normalized period for the varying fill factor. (a–c) The normalized groove depth of 0.5λ for TE polarization. (d–f) The normalized grove depth of 0.5λ for TM polarization. (g–i) The normalized groove depth of 1.0λ for TE polarization. (j–l) The normalized groove depth of 1.0λ for TM polarization.

For the specific case of the second order, SDT results are nearer to SF-FDTD in Figs. 5(c) and 5(f), being slightly better the prediction in TM polarization and for fill factors different from 0.5. Thus, the second-order diffraction analysis permits one to identify the phenomenon that SDT gives more accurate results for zeroth and first orders in different scenarios than for second order. While SDT accuracy for the zeroth order and both first orders is better with a fill factor of 0.5 this cannot be ensured for the second order.

Figure 6 shows the diffraction efficiency for the zeroth, first, and second orders for different periods and fill factors for both FDTD and SDT. The greater differences between theories are obtained for the specific case of $\Lambda/\lambda = 2$. For this case, the most accurate results are achieved with fill factors of 0.5 and smaller depths ($h/\lambda \leq 0.5$). As the grating period becomes greater, the similarity between FDTD and SDT is clearly manifested, the most accurate prediction being by SDT also with $f = 0.5$ for the zeroth and first orders. However, it is interesting to identify how the results shown in Figs. 6(b), 6(d), and 6(f) exhibit the best precise curves by SDT and also provide the worst predictions for the second order. In this cases, SDT sets the amplitude of the second order to zero; however, it can be seen that the real amplitude of this order in some cases reaches an efficiency of the 10% and is totally neglected by SDT.

The same analysis has also been carried out for TM polarization obtaining similar results to those given by TE polarization in Fig. 7. As mentioned below, the best performance with SDT for the zeroth and first orders is always achieved with low-spatial frequency gratings and for $f = 0.5$. With these parameters, the diffraction efficiency predicted by SDT is quite close to those obtained by FDTD, being more accurate for the first than for the zeroth order. The second order provided by SDT is close to FDTD results for duty cycles different from 50%.

4.2 *Validation of the Anisotropic Version*

For validating the anisotropic version, a polarization grating with the same characteristics detailed in the work of Oh et al.[3] has been considered. The validation of this system gives us the opportunity for extrapolating this formalism to other optical devices such as TN-LC or parallel-aligned LCoS. In this case, the periodic anisotropic structure varies along the x-direction with the following structure:

$$\epsilon(x) = \begin{bmatrix} n_\perp^2 \cos^2\alpha + n_{||}^2 \sin^2\alpha & (n_\perp^2 - n_{||}^2)\sin\alpha\cos\alpha & 0 \\ (n_\perp^2 - n_{||}^2)\sin\alpha\cos\alpha & n_\perp^2 \sin^2\alpha + n_{||}^2\cos^2\alpha & 0 \\ 0 & 0 & n_\perp^2 \end{bmatrix}, \tag{9}$$

where $\epsilon_{1,3} = n_\perp^2$, $\epsilon_2 = n_{||}^2$, $\alpha(x) = \pi x/\Lambda$, and $\beta = \gamma = 0$. The material parameters are $n_\perp = 1.5$, $n_{||} = 1.7$, and $\Delta n_l = n_{||} - n_\perp = 0.2$. In addition, gradient-index anti-reflection coatings are applied in air-PG boundaries.[3,54]

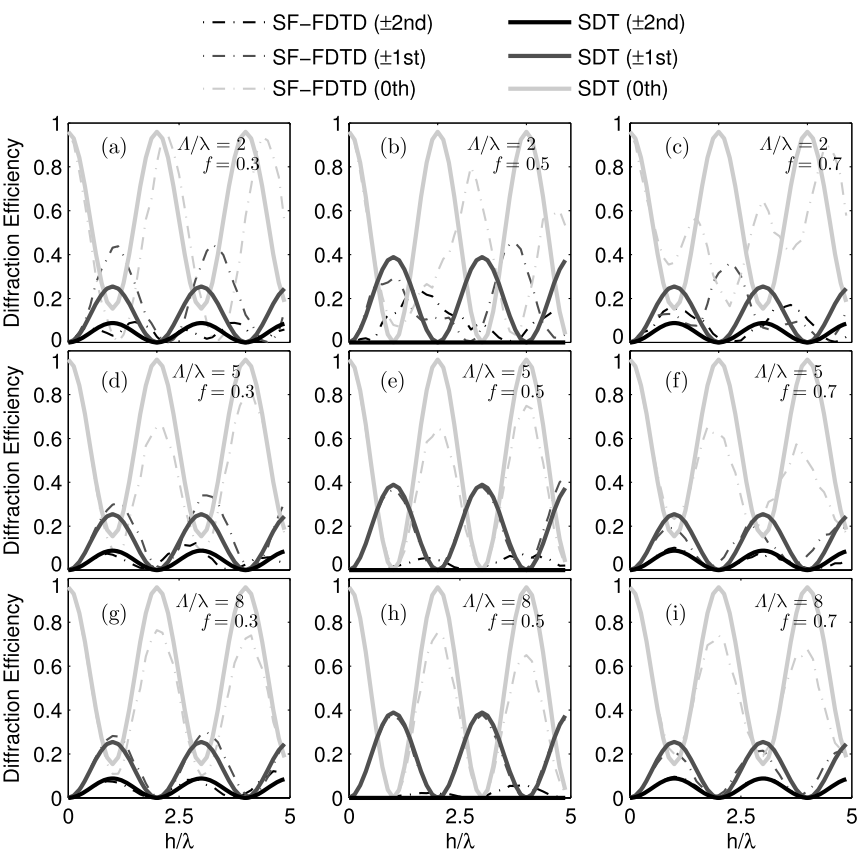

Fig. 6 Comparison of transmittance characteristic between the scalar method and FDTD for the 0th, ±1, and ±2 orders as a function of the normalized groove depth at normal incidence for TE polarization. (a–c) For $\Lambda/\lambda = 2.0$ at the fill factors of 0.3, 0.5, and 0.7. (d–f) For $\Lambda/\lambda = 5.0$ at the fill factors of 0.3, 0.5, and 0.7. (g–i). For $\Delta/\lambda = 8.0$ at the fill factors of 0.3, 0.5, and 0.7.

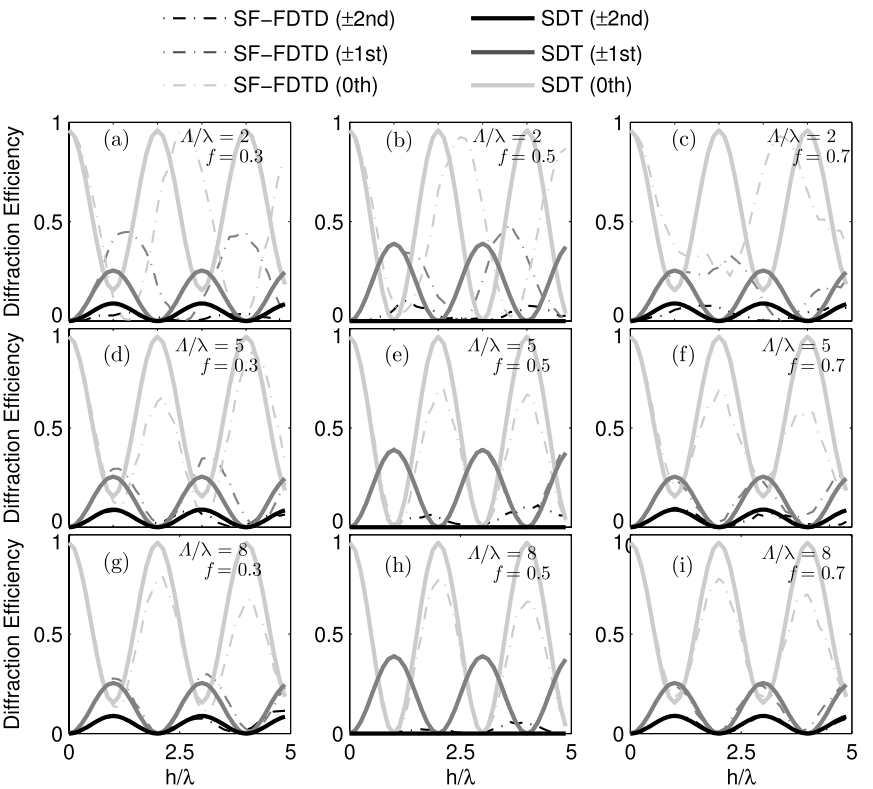

Fig. 7 Comparison of transmittance characteristic between the scalar method and FDTD for the 0th, ±1, and ±2 orders as a function of the normalized groove depth at normal incidence for TM polarization. (a–c): For $\Lambda/\lambda = 2.0$ at the fill factors of 0.3, 0.5, and 0.7. (d–f): For $\Lambda/\lambda = 5.0$ at the fill factors of 0.3, 0.5, and 0.7. (g–i). For $\Delta/\lambda = 8.0$ at the fill factors of 0.3, 0.5, and 0.7.

Figure 8(a) shows the near-field image of a PG captured from SF-FDTD. The accuracy of the SDT has been corroborated as a function of the parameters that define a binary phase grating. In order to verify the results obtained via these simplified theories, the SF-FDTD method has been considered for simulating periodic media. The results obtained here confirms the behavior of SDT applied to binary phase gratings detailed in Ref. 37 for the zeroth and first orders. In this article, the results of the second harmonic are also included and a full analysis of TE and TM polarization is also considered.

Regarding SDT, the results show that this theory is closer to SF-FDTD for greater normalized periods and for fill factors of 0.5, the accuracy of the results for the first order are quite better in all cases compared with those obtained for the zeroth order. The worst prediction of the second order is obtained for $f = 0.5$ which corresponds to the best situation for predicting the zeroth and first orders. The effect of the grating depth is also studied, finding that SDT behaves more precisely for thinner gratings with an equal grating period. In the analysis of the performance of the SDT as a function of the grating period, a slight improvement has been detected in the accuracy of the results for TM polarization that is usually more difficult to analyze with Fourier modal method (FMM) or RCWA schemes. Here, SF-FDTD is proposed as an alternative to those numerical methods usually applied in periodic media such as FMM and RCWA. These methods exhibit lower convergence ratios for TM polarization and more difficulties than finite-difference approaches in adapting their schemes for different types of media.

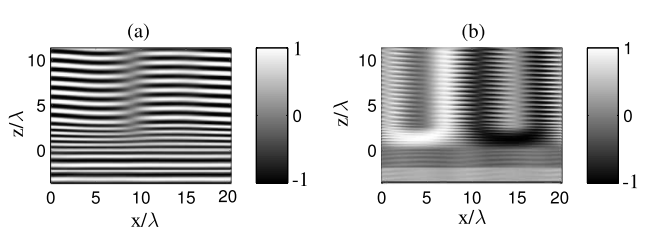

Fig. 8 Polarization grating analysis for normal incidence. (a) Near-field image of the E_x field as a function of the grid size. (b) S_3 Stokes parameter.

It can be identified how the polarization grating provides circular polarization with both senses right and left at the output plane. This effect can be easily identified by means of the representation of the S_3 Stokes parameter in Fig. 8(b). These results are consistent with those detailed in previous works.[3]

In order to validate the library here, also implemented in nonnormal incidence, a similar analysis has been performed varying the angle of incidence of the input plane wave. The new angle of incidence is $\theta_0 = 10$ deg, and the E_x and the S_3 Stokes parameter are also represented in Figs. 9(a) and 9(b), respectively. This results are consistent with those obtained in Fig. 8, and thus validate our implementation for anisotropic media.

4.3 *Computational Performance*

A set of simulations with both the isotropic and the anisotropic versions have been performed. In order to compare both scenarios, the time simulation costs have been compared for the analysis of a binary dielectric grating for the

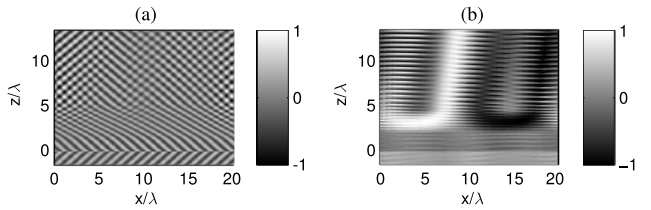

Fig. 9 Polarization grating analysis for oblique incidence ($\theta_0 = 10°$). (a) Near-field image of the E_x field as a function of the grid size. (b) S_3 Stokes parameter.

isotropic version and a phase grating for the anisotropic version. In both cases, the time costs of the CPU and GPU versions are compared as a function of the grid size. The variation of the grid size has been established by means of the density parameter R that has been modified from $R = 10$ to $R = 400$. Figure 10 shows the SpeedUp, defined as T_{CPU}/T_{GPU} for both versions implemented as a function of the grid size in MCells. The number of steps of each simulation has also been modified in order to ensure the steady state in all cases. For the specific case of GPU computing, the time measurements shown here also include the time that GPU invests in downloading the field components into the host memory. The authors consider that this process is inherent to GPU computing, and it also must be considered for accurately measuring the degree of improvement of this platform.

As can be seen in Fig. 10(a), the SpeedUp has a rapidly upward trend for both versions as the simulation size becomes greater. This trend is modified for bigger simulation sizes and remains close to a upper limit. For the isotropic GPU implementation, a factor near to 15 is achieved in the best cases, whereas the anisotropic version with GPU computing is more than 22 times faster than the CPU version. Figure 10(b) represents the time simulation costs for the isotropic and nonisotropic media for both platforms and different thicknesses of the anisotropic layer. A dramatic growth of the time-costs' requirements for the nonisotropic version can be easily identified in this graph, reaching values of almost 30 h for the biggest simulation size considered here. Nevertheless, the GPU time costs for both kind of problems remain under 3 h in the worst case.

5 Conclusions

In this work, the SF-FDTD for the analysis of anisotropic periodic media has been accelerated by means of GPU computing. First, the isotropic version has been implemented in CPU and also in GPU, and its potential has been corroborated by means of a deep analysis of the diffraction efficiency of binary phase gratings. The accuracy of the SDT has been corroborated as a function of the parameters that define a binary-phase grating. The results obtained here confirm the behavior of SDT applied to binary phase gratings detailed in Ref. 37 for the zeroth and first orders. In this article, the results of the second harmonic are also included, and a full analysis of TE and TM polarization is also considered. Regarding SDT, the results showed that this theory is closer to SF-FDTD for greater normalized periods and for fill factors of 0.5. The accuracy of the results for the first order are quite better in all cases compared with those obtained for the zeroth order. The worst prediction of the second order is obtained for $f = 0.5$ that corresponds to the best situation for predicting the zeroth and first orders. This analysis permits one to conclude that SF-FDTD is a powerful approach to be used for the analysis of DOEs, where the simplified theories show that they are not accurate enough. The GPU implementation proposed here makes more competitive the SF-FDTD approach compared with analytical closed solutions.

Second, the anisotropic version has also been validated by means of the study of the near-field pattern, and the Stokes parameters of a polarization grating also achieving good results, thus validating the implementation described here. The computational results are based on the analysis of the SpeedUp obtained as the difference of the sequential and the parallel simulation times and also of the time-cost values. This analysis has been performed as a function of the grid simulation size for both isotropic and anisotropic media cases. The degree of improvement of the isotropic GPU version is nearly 15 compared with the CPU version, whereas the anisotropic GPU version of the library provides better values of the SpeedUp, being nearer to 22 times faster than the CPU version. These results join the values of the time-run simulation for anisotropic media, which demonstrates that considering acceleration techniques for the anisotropic formulation of the SF-FDTD is mandatory for massive

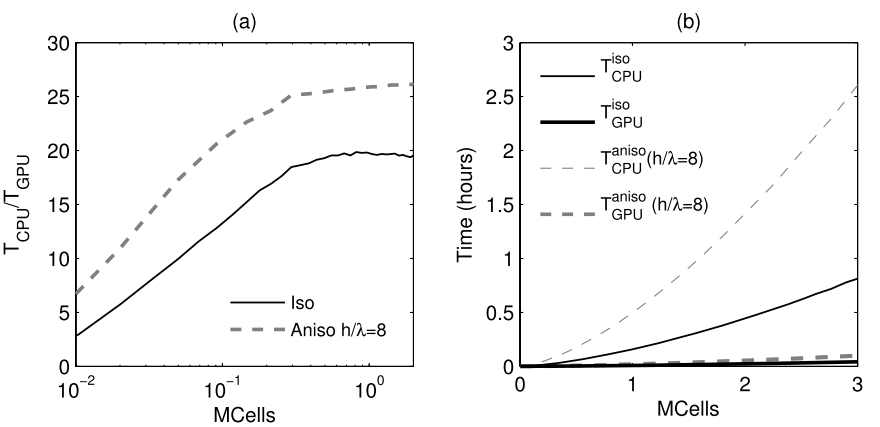

Fig. 10 Computational results. (a) SpeedUp of the isotropic and the anisotropic versions of SF-FDTD as a function of the grid size. (b) Time simulation costs as a function of the grid size.

computations. The SF-FDTD formalism in its anisotropic form requires considering all the field components, a full-tensor formulation of the dielectric permittivity, and complex notation. This last factor increases dramatically the number of operations and the complexity of the calculus of the method, degrading the performance in CPU computing. The authors are currently working in optimization techniques based on improving the performance in modern multicore CPU by means of shared memory approaches. Moreover, the authors are considering to improve the GPU implementation considering tiling techniques and more complex memory strategies, since the memory requirements of the anisotropic SF-FDTD can degrade the performance due to the limiting factor of memory in GPUs.

Acknowledgments

This work was supported by the Ministerio de Economía y Competitividad of Spain under projects FIS2011-29803-C02-01 and FIS2011-29803-C02-02 and by the Generalitat Valenciana of Spain under projects PROMETEO/2011/021, ISIC/2012/013, and GV/2012/099.

References

1. A. Taflove and S. C. Hagness, *Computational Electrodynamics: The Finite-Difference Time-Domain Method*, 2nd ed., Artech House, Boston (2000).
2. J. A. Roden et al., "Time-domain analysis of periodic structures at oblique incidence: orthogonal and nonorthogonal FDTD implementations," *IEEE Trans. Microwave Theory Tech.* **46**(4), 420–427 (1998).
3. C. Oh and M. J. Scuti, "Time-domain analysis of periodic anisotropic media at oblique incidence: an efficient FDTD implementation," *Opt. Express* **14**(24), 11870–11884 (2006).
4. M. N. Miskiewicz, P. T. Bowen, and M. J. Escuti, "Efficient 3D FDTD analysis of arbitrary birefringent and dichroic media with obliquely incident sources," *Proc. SPIE* **8255**, 82550W (2012).
5. D. B. Kirk and W. W. Hwu, *Programming Massively Parallel Processors: A Hands-on Approach*, Morgan Kaufmann, Burlington (2010).
6. J. Sanders and E. Kandrot, *CUDA by Example: An Introduction to General-Purpose GPU Programming*, Addison-Wesley, Upper Saddle River (2010).
7. M. Bernaschi, G. Parisi, and L. Parisi, "Benchmarking GPU and CPU codes for Heisenberg spin glass over-relaxation," *J. Comput. Phys. Commun.* **182**(6), 1265–1271 (2011).
8. N. Ferrando et al., "Octree-based, GPU implementation of a continuous cellular automaton for the simulation of complex, evolving surfaces," *Comput. Phys. Commun.* **182**(3), 628–640 (2011).
9. E. B. Ford, "Parallel algorithm for solving Keplers equation on graphics processing units: application to analysis of Doppler exoplanet searches," *New Astron.* **14**(4), 406–412 (2009).
10. C. Harris, K. Haines, and L. Staveley-Smith, "GPU accelerated radio astronomy signal convolution," *Exp. Astron.* **22**(1–2), 129–141 (2008).
11. S. Bianchi and R. Di Leonardo, "Real-time optical micro-manipulation using optimized holograms generated on the GPU," *J. Comput. Phys. Commun.* **181**(8), 1444–1448 (2010).
12. X. Gu et al., "Implementation and evaluation of various demons deformable image registration algorithms on a GPU," *Phys. Med. Biol.* **55**(1), 207–219 (2010).
13. D. Gross et al., "GPU-based volume reconstruction from very few arbitrarily aligned X-ray images," *SIAM J. Sci. Comput.* **31**(6), 4204–4221 (2009).
14. Z. A. Taylor et al., "On modelling of anisotropic viscoelasticity for soft tissue simulation: numerical solution and GPU execution," *Med. Image Anal.* **13**(2), 234–244 (2009).
15. C. Trapnell and M. C. Schatz, "Optimizing data intensive GPGPU computations for DNA sequence alignment," *Parallel Comput.* **35**(8–9), 429–440 (2009).
16. C.-T. Yang, C.-L. Huang, and C. F. Lin, "Hybrid CUDA, OpenMP, and MPI parallel programming on multicore GPU clusters," *J. Comput. Phys. Commun.* **182**(1), 266–269 (2011).
17. A. Shahmansouri and B. Rashidian, "GPU implementation of split-field finite difference time-domain method for Drude-Lorentz dispersive media," *Prog. Electromagn. Res.* **125**, 55–77 (2012).
18. T. Kämpfe and O. Parriaux, "Depth-minimized, large period half-wave corrugation for linear to radial and azimuthal polarization transformation by grating-mode phase management," *J. Opt. Soc. Am. A* **28**(11), 2235–2242 (2011).
19. A. Mellor et al., "A numerical study of bi-periodic binary diffraction gratings for solar cell applications," *Sol. Energ. Mat. Sol. C.* **95**(12), 3527–3535 (2011).
20. N. Nguyen-Huu, Y.-B. Chen, and Y.-L. Lo, "Development of a polarization-insensitive thermophotovoltaic emitter with a binary grating," *Opt. Express* **20**(6), 5882–5890 (2012).
21. M. Lõhmus et al., "Diffraction of ultrashort optical pulses from circularly symmetric binary phase gratings," *Opt. Lett.* **37**(7), 1238–1240 (2012).
22. C.-Y. Chen et al., "Binary blazed grating based on autostereoscopic display mechanism," *Appl. Opt.* **51**(7), 877–882 (2012).
23. G. Bloom et al., "Passive coherent beam combining of quantum-cascade lasers with a Dammann grating," *Opt. Lett.* **36**(19), 3810–3812 (2011).
24. L. García-Martínez, R. Rosete-Aguilar, and J. Garduño-Mejia, "Gauss-Legendre quadrature method used to evaluate the spatio-temporal intensity of ultrashort pulses in the focal region of lenses," *Appl. Opt.* **51**(3), 306–315 (2012).
25. L. Changhai et al., "Performance analysis of multiplexed phase computer-generated hologram for modal wavefront sensing," *Appl. Opt.* **50**(11), 1631–1639 (2011).
26. X. J. Wang et al., "Angle-resolved reflectance of obliquely aligned silver nanorods," *Appl. Opt.* **51**(10), 1521–1531 (2012).
27. H. Zhang et al., "Effective medium theory for random media composed of two-layered spheres," *J. Opt. Soc. Am. A Optic. Image Sci. Vis.* **28**(11), 2292–2297 (2011).
28. G. R. Harrison, "The production of diffraction gratings: I. Development of the ruling art," *J. Opt. Soc. Am.* **39**(6), 413–426 (1949).
29. G. R. Harrison, "The production of diffraction gratings: II. The design of echelle gratings and spectrographs," *J. Opt. Soc. Am.* **39**(7), 522–528 (1949).
30. M. Nevière, "Electromagnetic versus scalar theory for modeling diffraction gratings: is electromagnetic modeling necessary for practical applications?," *Proc. SPIE*, **2532**, 362–373 (1995).
31. D. L. Brundrett, E. N. Glytsis, and T. K. Gaylord, "Homogeneous layer models for high-spatial-frequency dielectric surface-relief gratings: conical diffraction and antireflection designs," *Appl. Opt.* **33**(13), 2695–2706 (1994).
32. E. N. Glytsis and T. K. Gaylord, "High-spatial-frequency binary and multilevel stairstep gratings: polarization-selective mirrors and broadband antireflection surfaces," *Appl. Opt.* **31**(22), 4459–4470 (1992).
33. C. W. Haggans and L. Lifeng, "Effective-medium theory of zeroth-order lamellar gratings in conical mountings," *J. Opt. Soc. Am. A* **10**(10), 2217–2225 (1993).
34. D. A. Pommet, M. G. Moharam, and E. B. Grann, "Limits of scalar diffraction theory for diffractive phase elements," *J. Opt. Soc. Am. A* **11**(6), 1827–1834 (1994).
35. E. N. Glytsis, "Two-dimensionlly-periodic diffractive optical elements: limitations of scalar analysis," *J. Opt. Soc. Am. A* **19**(4), 702–715 (2002).
36. D. A. Pommet, M. G. Moharam, and E. B. Grann, "Limits of scalar diffraction theory for diffractive phase elements," *J. Opt. Soc. Am. Optic. Image Sci. Vis.* **11**(6), 1827–1834 (1994).
37. X. Jing and Y. Jin, "Transmittance analysis of diffraction phase grating," *Appl. Opt.* **50**(9), C11–C18 (2011).
38. C. Dissanayake et al., "FDTD modeling of anisotropic nonlinear optical phenomena in silicon waveguides," *Opt. Express* **18**(20), 21427–21448 (2010).
39. I. W. Hsieh et al., "Cross-phase modulation-induced spectral and temporal effects on co-propagating femtosecond pulses in silicon photonic wires," *Opt. Express* **15**(3), 1135–1146 (2007).
40. T. Liang et al., "Ultrafast all-optical switching by cross-absorption modulation in silicon wire waveguides," *Opt. Express* **13**(19), 7298–7303 (2005).
41. Q. Lin et al., "Ultrabroadband parametric generation and wavelength conversion in silicon waveguides," *Opt. Express* **14**(11), 4786–4799 (2006).
42. Y.-H. Kuo et al., "Demonstration of wavelength conversion at 40 Gb/s data rate in silicon waveguides," *Opt. Express* **14**(24), 11721–11726 (2006)
43. H. Fukuda et al., "Four-wave mixing in silicon wire waveguides," *Opt. Express* **13**(12), 4629–4637 (2005).
44. Q. Xu, V. R. Almeida, and M. Lipson, "Demonstration of high Raman gain in a submicrometer-size silicon-on-insulator waveguide," *Opt. Lett.* **30**(1), 35–37 (2005).
45. S.-D. Wu and E. N. Glytsis, "Finite-number-of-periods holographic gratings with finite-width incident beams: analysis using the finite-difference frequency-domain method," *J. Opt. Soc. Am. A* **19**(10), 2018–2029 (2002).
46. A. D. Papadopoulos and E. N. Glytsis, "Finite-difference-time-domain analysis of finite-number-of-periods holographic and surface-relief gratings," *Appl. Opt.* **47**(12), 1981–1994 (2008).
47. K. S. Yee, "Numerical solution of initial boundary value problems involving Maxwell's equations in isotropic media," *IEEE Trans. Antennas Propag.* **14**(3), 302–307 (1966).

48. J. Francés et al., "Rigorous interference and diffraction analysis of diffractive optic elements using the finite-difference time-domain method," *Comput. Phys. Commun.* **181**(12), 1963–1973 (2010).
49. G. B. Arfken and H. J. Weber, *Mathematical Methods for Physicists*, 4th ed., Academic Press, San Diego (1995).
50. J. Francés et al., "Performance analysis of the FDTD method applied to holographic volume gratings: multi-core CPU versus GPU computing," *Comput. Phys. Commun.* **184**(3), 469–479 (2013).
51. J. Francés et al., "Comparison of simplified theories in the analysis of the diffraction efficiency in surface-relief gratings," *Proc. SPIE* **8429**, 84291U (2012).
52. T. Hoshino et al., "Diffraction pattern of triangular grating in the resonance domain," *J. Opt. Soc. Am. A* **26**(3), 715–722 (2009).
53. J. C. Cowan, "Aztec surface-relief volume diffractive structure," *J. Opt. Soc. Am. A* **7**(8), 1529–1544 (1990).
54. W. H. Southwell, "Gradient-index anti-reflection coatings," *Opt. Lett.* **8**(11), 584–586 (1983).

Jorge Francés received the PhD degree at the University of Alicante in 2011. He received his MSEE in 2009 and his BSEE in 2006, both from the Technical University of Valencia, Valencia, Spain. He has been working as an assistant lecturer with the University of Alicante since 2008. His main research interests include physical optics, sound and vibration, and numerical simulation.

Sergio Bleda Perez received the Ingeniero degree in computer science (1999) and Ingeniero Técnico degree in telecommunications (2002) from the University of Alicante, and a PhD in telecommunications (2009) from the Polytechnic University of Valencia. He has been working as a professor at the University of Alicante since 2000. His current research interests are the optimization of numerical methods for both optics and acoustics.

Mariela Lázara Álvarez received her BS degree in physics from Havana University in 1994, and PhD in science by Alicante University in 2001 in particle optical characterizations. Currently she is professor in the Department of Physics, System Engineering and Signal Theory, and a researcher in the Institute of Physics Applies to Sciences and Technologies in Alicante University. Her research interests include the holographic register materials, processed and optical storage of information, the study and characterization of liquid glass screens, and the theoretical models of electromagnetic radiation propagation in periodic means.

Francisco Javier Martínez received his BS degree in electronic engineering from University of Valencia in 1996 and his BS degree in physics in 1999. Currently, he is a research assistant with the Applied Physics to Science and Technology Institute from University of Alicante, and assistant professor of electronics in Miguel Hernandez University. His research interests include difractive optics and holography.

Andrés Márquez completed his physics degree at the Universidad Autónoma de Barcelona, Spain, in 1996, and received his MSc and PhD degrees in physics in the Department of Physics, Group of Optics, Universidad Autónoma de Barcelona, in 1997 and 2001, respectively. In 2000 he joined the Group of Holographic Materials in the Universidad de Alicante, where he is a professor of applied physics. His research interests include holographic recording materials, liquid crystal spatial light modulators, optical image processing and diffractive optics.

Cristian Neipp received the MS degree in physics from the University of Salamanca, Salamanca, Spain, in 1996, and the PhD degree in physics from the University of Alicante, Alicante, Spain, in 2001. He has taught applied physics for engineering students since 1998. Since 2002, he has been a permanent whole-time lecturer of applied physics with the University of Alicante. He is mainly interested in holography, holographic recording materials, holographic optical elements, optical processing, electromagnetic theory of diffraction and volume gratings, and physics and engineering education. In these areas, he has published more than 130 technical papers in various journals and presented more than 100 papers in scientific conferences and congresses.

Augusto Beléndez received his MSc degree in physics and PhD degree in physics (summa cum laude) from the University of Valencia, Spain, in 1986 and 1990, respectively. He has taught applied physics for engineering students since 1986. In 1996 he became full professor of applied physics at the University of Alicante. He is mainly interested in holography, holographic recording materials, holographic optical elements, optical processing, nonlinear oscillations and the teaching of physics and engineering. In these areas he has published more than 250 technical papers in various journals and presented more than 210 papers in scientific conferences and congresses. Between 1993 and 2007 he was the head of the Department of Physics, Systems Engineering and Signal Theory at the University of Alicante, Spain, and in 2009 was appointed head of the Research Institute of Physics Applied to Sciences and Technologies at the same university. He is a member of the board of editors of the International Journal of Engineering Education, Advances in Optical Technologies and the International Journal of Optics. He is a member of the Spanish Optical Society (SEDOPTICA), Royal Spanish Society of Physics (RSEF) and European Optical Society (EOS). He is senior member of the SPIE and the Optical Society of America (OSA).